RESEARCH PAPER

Synthesis of Fe-TiC Hard Coating From Ilmenite Via Laser Cladding

A. Khalili[1], M. Mojtahedi[*2], M. Goodarzi[3] and M. J. Torkamany[4]

** m.mojtahedi@razi.ac.ir*

Received: June 2018 **Revised: December 2018** **Accepted: May 2019**

[1] Alumni; School of Metallurgy and Materials Engineering, Iran University of Science and Technology, Tehran, Iran.
[2] Assistant professor; Department of Materials and Textile Engineering, Razi University, Kermanshah, Iran.
[3] School of Metallurgy and Materials Engineering, Iran University of Science and Technology, Tehran, Iran.
[4] Iranian National Center for Laser Science and Technology, Tehran, Iran.

DOI: 10.22068/ijmse.16.2.79

Abstract: *The aim of this work was to synthesize TiC reinforced coating on carbon steel via reduction of ilmenite powder. A mixture of ilmenite and graphite was pre-placed on AISI 1020 steel surface. The effect of the addition of excess graphite amounts on the progress of the synthesis of carbide particles was studied. The evolution of phases in different coatings was analyzed via X-ray diffraction and scanning electron microscopy. Then, the initial powder mixtures were mechanically activated for various durations, to accelerate the reactions in the transient melt pool. Finally, the Fe-TiC hard coating was successfully synthesized by carbothermic reduction of ilmenite through laser surface treatment. Moreover, it is proved that combination of mechanical activation with additive laser melting effectively improves the level of ilmenite reduction, besides enhancing the distribution of hard particles and the hardness of the coatings to more than 1300 HV.*

Keywords: *laser surface treatment, cladding, hard coating, TiC particles, carbothermic reduction.*

1. INTRODUCTION

Synthesis of hard coatings on metallic substrates is a typical way to take advantage of the hardness of ceramic reinforcements besides preserving toughness of bulk metallic materials. Application of various hard ceramic particles such as TiC, TiB2, WC, TiN, B4C, VC, SiC, and Al2O3 has been studied [1, 2]. It is claimed that titanium carbide is a suitable reinforcing particle for iron-based alloys. TiC particles have high hardness, high melting point, low density, appropriate wettability, and also chemical stability in iron [3]. Moreover, the Fe-TiC metal matrix composites (MMC) show attractive functional properties such as high wear resistance [4], high tensile strength [5], and proper ductility [6].

Several production methods are proposed and developed for the fabrication of Fe-TiC MMC as a hard coating. The majority of methods apply high temperature, including laser cladding [7], plasma cladding [8, 9], HVOF [10, 11], high-energy electron beam [12], Tungsten-inert gas (TIG) [13, 14], and reactive flame spraying [15]. However, the laser beam has special features as a heat source, including high automation ability, cleanness of the process, and low energy input which results in little distortion and relatively narrow heat-affected zone. The laser beam also forms a melt pool which spreads to the substrate and creates a metallurgical bond [16].

On the other hand, MMC coatings can improve the resistance of low-cost materials to operational damages such as corrosion and wear. Coatings containing TiC particles have been applied to various substrates via laser cladding. The substrate which has attracted the most interest is steel, that is much cheaper than other candidates e.g. Ni-based superalloys [17, 18] or commercially pure titanium [19]. Then again, the TiC particles can be synthesized in-situ in a surface melt pool. The process has been performed on steel substrates by the application of elemental powder mixtures such as Ti + graphite [20] or Ti + Fe + graphite [21]. A further step was a direct in-situ synthesis of TiC from ferrotitanium + graphite, instead of applying

[Downloaded from transjour.iust.ac.ir on 2025-05-28]

[DOI: 10.22068/ijmse.16.3.75]

elemental Ti powder [7, 22]. The production of Fe-TiC surface coatings from minerals of titanium is a more complex process. The short heating time of LST may be insufficient to complete the steps of minerals reduction. On the other hand, such a process is cost-effective due to the utilization of cheaper raw materials.

Some investigations were performed on the production of bulk or powder Fe-TiC MMC by the reduction of ilmenite (FeTiO3) via different methods [23-25]. However, to the best of the author's knowledge, no other work has been published about the synthesis of the Fe-TiC coating by the reduction of ilmenite via LST. Therefore, the aim of the present research is to fabricate in-situ Fe-TiC MMC coating via carbothermic reduction of inexpensive raw materials. A pulsed laser beam is used to trigger the reactions between graphite and ilmenite. It is reported that about 30 minutes is required for the reduction of ilmenite powder by graphite at 1673 K (1400°C) [26], which is much higher than the time duration of LST. Therefore two solutions were applied in this research, which may facilitate the reduction process. Firstly, the effects of the addition of excess carbon content were examined. Secondly, the precursor powders were mechanically activated. The resulted variations in synthesis routes and phase transformations are technically discussed.

2. EXPERIMENTAL PROCEDURE

Graphite (<5 μm size, from Merck KGaA) and ilmenite (<100 μm size, from AMA Industrial Co.) powders were used. The iron and titanium contents of the ilmenite were measured via wet chemistry analysis, which were 30.71 wt % and 32.19 wt %, respectively. According to the equation (1), in a stoichiometric condition, four moles of carbon are needed for the reduction of one mole of ilmenite to iron and titanium carbide [3]:

$$FeTiO_{3(s)} + 4C_{(gr)} = Fe_{(s)} + TiC_{(s)} + 3CO_{(g)}\ ,$$
$$\Delta G^{\circ}=662.6–47.9\ T\ \ (KJ) \qquad (1)$$

In which G° is standard Gibbs free energy and T is the temperature in Kelvin. The applied graphite/ilmenite molar ratios and milling times are presented in table 1. The powders were mechanically activated at room temperature in an attritor ball mill with hardened steel jar and balls. Ball to powder weight ratio and rotational speed were set at 15:1 and 160 rpm, respectively. After ball milling, the blended powders were mixed with an equal weight of polyvinyl alcohol in an ultrasonic bath. The resultant suspensions were placed on 70×40×5 mm AISI 1020 steel substrates. The thickness of the preplaced layers was 0.5 mm. Afterward, the specimens were dried at 110 °C for 60 minutes.

A 400 W Nd:YAG pulsed laser (model IQL-10) was used as the heat source. The properties of the laser beam were as follows: 225 W laser power, 15 J pulse energy, 10 milliseconds pulse duration, and 15 Hz frequency. The beam scanning speed was 2 mm/s. Moreover, the laser spot size on the surface of workpiece was 1.5 mm and overlapping of adjacent laser tracks was 30%. During the process, high purity argon gas (99.999 %) was supplied through a nozzle at the rate of 20 liters per minute.

After laser treatment, the coated specimens were sectioned vertically, ground with SiC paper,

Table 1. The applied graphite/ilmenite molar ratios and mechanical activation times.

Sample	Graphite/ilmenite molar ratio	Milling time (hours)
4-100	4	100
6-100	6	100
8-100	8	100
8-5	8	5
8-50	8	50
8-200	8	200

[Downloaded from transjour.iust.ac.ir on 2025-05-28]

[DOI: 10.22068/ijmse.16.3.75]

polished with a fine alumina powder suspension and were subsequently etched by 3% nital solution. The microstructures of samples were studied using scanning electron microscopy (SEM) and energy dispersed spectrometry (EDS). X-ray diffraction (XRD) analyses were also used to track microstructural and phase evolutions. A Philips X-ray diffractometer with CuKα radiation was used under the voltage and current of 40 kV and 30 mA, respectively. Lastly, microhardness measurements were performed using a Vickers microhardness apparatus with a normal load of 100 grams.

3. RESULTS AND DISCUSSION

Firstly, the effect of carbon/ilmenite ratio on the synthesis of TiC particles was investigated. The powders with 100 hours of mechanical activation were applied. After that, the desired carbon to ilmenite molar ratio was fixed and the effect of activation time was studied. It should be mentioned that the microstructural aspects of the final coating were described in details in another article [27]. The effects of heat input and laser parameters on the microstructure and properties of the coating will be published elsewhere.

3.1. The effect of carbon/ilmenite molar ratio on the microstructure of the coating

The conducted phase evolutions were firstly investigated by microscopic study of the developed microstructures. An intersection of the sample that is synthesized under stoichiometric carbon/ilmenite ratio is shown in Fig. 1.a. The surface, coated region and HAZ can be recognized. As can be seen in Fig. 1.b, a martensitic structure is formed in the matrix of coating, which can be due to the increased carbon content of the substrate. Some particles were also analyzed via EDS. For instance, it is observed that the particle marked by an arrow in Fig. 1.b, contained titanium and oxygen, while oxygen was absent in some other particles. Dewan et al [28] showed that carbothermic reduction of ilmenite results in the consecutive formation of TiO2, Ti3O5, Ti2O3 and finally TiC. Therefore, a primary conclusion is that the visible particles in our study are combinations of oxide and carbide phases. It should be mentioned that the carbon atoms could not be well detected via EDS analysis. Moreover, a martensitic structure is formed in the matrix of coating (Fig. 1.c). This can be a consequence of the fast cooling rate of the melt pool and the increase of the carbon content of the mild steel substrate. The observation is also in agreement with a research on the in-situ synthesis of TiC-VC hardened coating using ferroalloys and graphite [29].

The coating and HAZ regions of sample 6-100 can be observed in Fig. 2.a. Similar to sample 4-100, the HAZ region may have a bainitic/acicular ferritic structure. As is depicted in the titanium elemental map, in the lower part of Fig. 2.a, several particles which contain titanium were dispersed in the coated region. An area with the accumulation of particles is pointed by an arrow. A back-scattered electron image of this area is displayed in Fig. 2.b. It should be mentioned that various particles in the BSE image have diverse

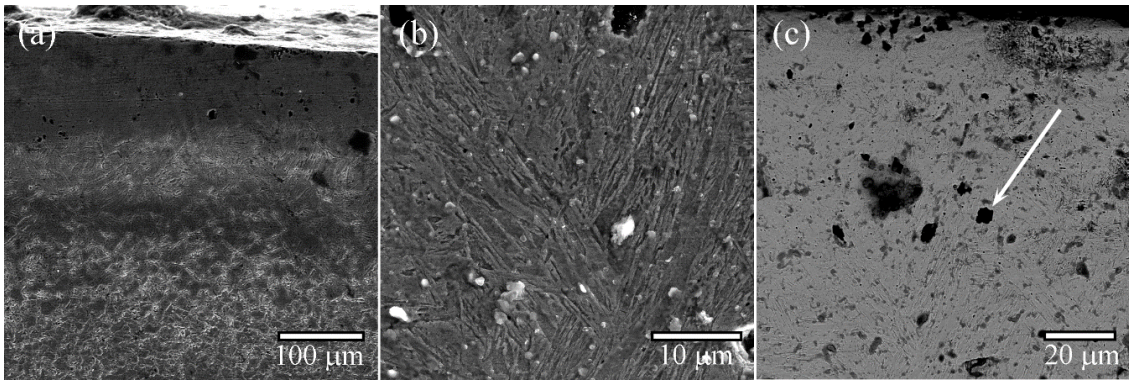

Fig. 1. SEM images of sample 4-100 (a) The overall structure of the surface layer
(b) The martensitic plates in the matrix of coating (c) BSE image of the coating and embedded particles

[Downloaded from transjour.iust.ac.ir on 2025-05-28]

[DOI: 10.22068/ijmse.16.3.75]

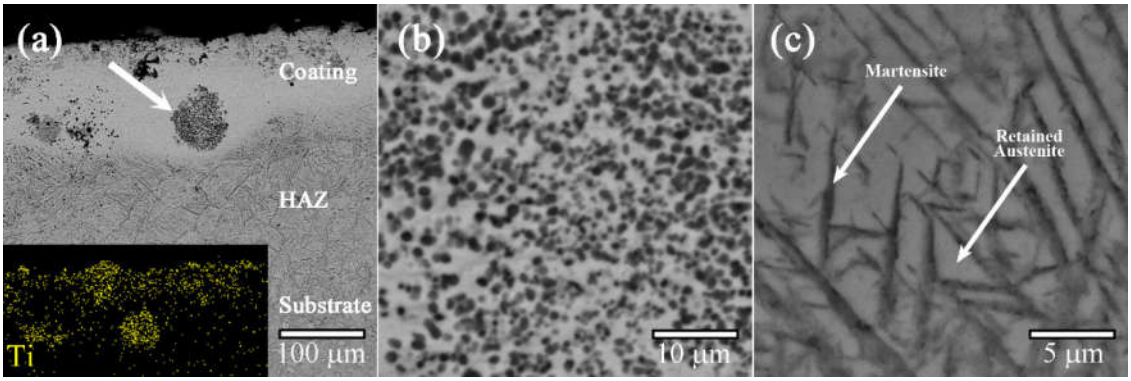

Fig. 2. BSE image of sample 6-100 (a) An intersection of the surface layer. The EDS map of titanium element in the clad layer is also presented. (b) An area of accumulation of synthesized particles, which was pointed by an arrow in the previous part; (c) Martensitic plates and retained austenite

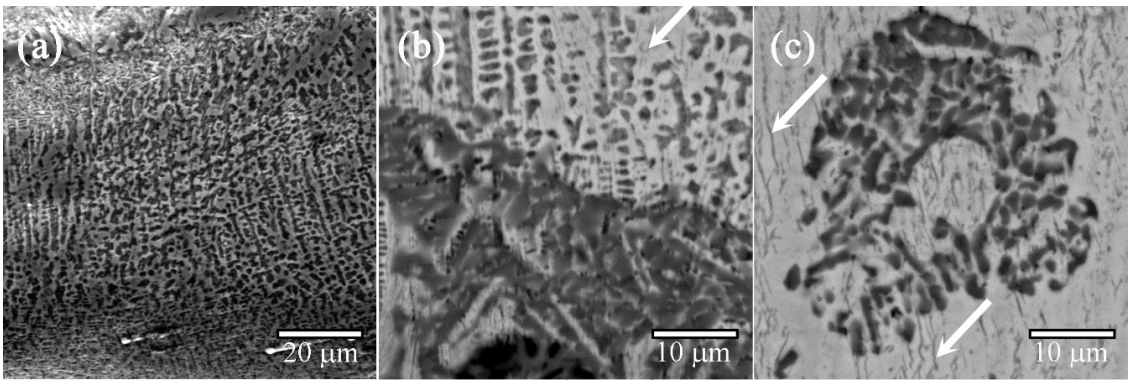

Fig. 3. SEM images of sample 8-100 (a) The formation of dendritic microstructure in the matrix (b) dendrites and inter-dendritic sections, besides some agglomerated particles (c) A cluster of synthesized particles embedded in the matrix of the coating

levels of darkness. The darker a particle's image, it may have a higher amount of the light element of carbon. Consequently, the coating can contain a mixture of particles which were reduced to different levels. Moreover, the matrix of the coated region is shown in Fig. 2.c. Again, the formation of martensitic plates is obvious. The presence of retained austenite can signify the increase of carbon content in the matrix.

Fig. 3. exhibits major microstructural aspects of the specimen that was fabricated at the graphite/ilmenite molar ratio of 8. As indicated in Fig. 3.a, the matrix of laser-treated coating is solidified in a dendritic mode. According to the constitutional supercoiling theory [30], this can be a result of the increase of solute atoms (here carbon) in the melt pool. A similar effect has been recently reported [31] by the addition of up to 4 wt % of carbon+boron to a coating on carbon steel, with in-situ generated TiC particles. The effect of available carbon content on the matrix of coatings can be considered as a basic difference between the in-situ carbothermic reduction of TiC and the ex-situ laser cladding of TiC particles. Higher magnification images of dendrites and the embedded particles are presented in Figs 3.b and 3.c. A phase with the shape of fine layers can be observed in the matrix of coating, such as the ones that are pointed by arrows. These can be layers of Fe3C, as will be discussed later via XRD analysis. On the other hand, EDS analysis of particles in sample 8-100 did not show any oxide phase. It can be determined that complete reduction of ilmenite took place and the oxide phases were replaced by the carbides.

The XRD analyses were conducted to deepen

[Downloaded from transjour.iust.ac.ir on 2025-05-28]

[DOI: 10.22068/ijmse.16.3.75]

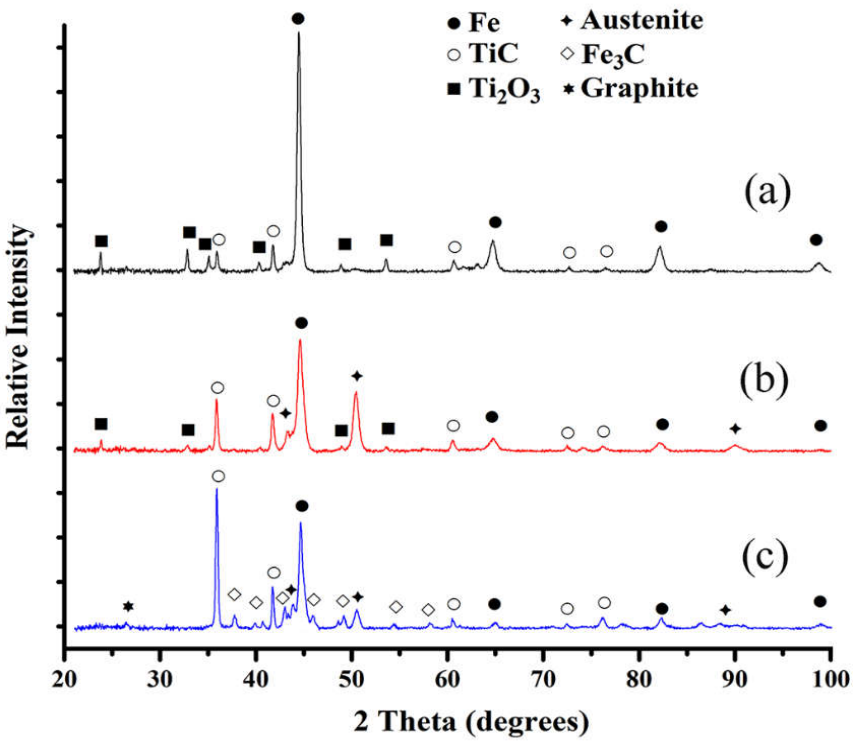

Fig. 4. XRD patterns of the samples by application of powder blends activated for 100 hours having different ilmenite to graphite molar ratios of (a) 4, (b) 6, (c) 8. Due to the difficulty of differentiating between the peaks of ferrite and martensite, the relevant peaks are labeled by Fe.

the study of phase transformations in the three molar ratios. As can be seen in Fig. 4.a, the formation of a mixture of oxide and carbide phases can be confirmed under the stoichiometric graphite content. It can be concluded that the amount of carbon is not sufficient to accomplish the steps of ilmenite carbothermic reduction, under the applied LST conditions. In comparison to sample 4-100, the height of the peaks of Ti2O3 was decreased in sample 6-100 (graphite/ilmenite molar ratio of 6). Alternatively, the presence of excess graphite resulted in an increase in the intensity of TiC peaks. According to the relative intensity of XRD lines, the amount of retained austenite in sample 6-100 was higher than 8-100 (Figs. 4.b and 4.c). On the other hand, the peaks of cementite emerged in the XRD profile of sample 8-100 and the higher carbon content resulted in the formation of more Fe3C and TiC. This is in agreement with SEM studies of sample 8-100.

It should be mentioned that the process of reduction in our study occurs in a liquid medium. Studies of finite element simulations of TiC laser cladding process calculated the temperature of the surface of melt to be 2810 °C [32], or even as high as 4500 °C [33]. The substance with the lowest melting point in this system is ilmenite. Therefore, the ilmenite particles firstly start to form a melt pool. Afterward, the pool will be diluted by iron from the substrate. Graphite with a melting point higher than 3500 °C [34] would be the last part to dissolve. A better understanding of the process can be achieved by the aid of Fe-Ti-C ternary phase diagram. As can be seen in Fig. 5 [35], the first phase which can be generated in the melt pool is TiC. By decreasing temperature, the amount of TiC increases until the composition of the melt pool reaches the triple point between TiC, δ-Fe, and γ-Fe. A prerequisite for the increase in TiC is a further reduction of ilmenite. If the composition of the melt becomes rich with titanium, the melt can cool down through path A in Fig. 5. But due to the supply of excess carbon from graphite, path B is more probable. In this way, more austenite will form. Afterward, this austenite can be transformed to martensite

[Downloaded from transjour.iust.ac.ir on 2025-05-28]

[DOI: 10.22068/ijmse.16.3.75]

or α+Fe3C. From the kinetic point of view, the increase of available carbon content can shorten the diffusion path. Sufficient graphite content can also provide enough reductant CO gas. On the other hand, it is stated that undissolved graphite particles can remain in the melt pool [20]. While free graphite particles were not detected in this work, unnecessary increase of graphite/ilmenite molar ratio to higher than 8 may result to leave undissolved graphite particles and damage the mechanical properties of the coating.

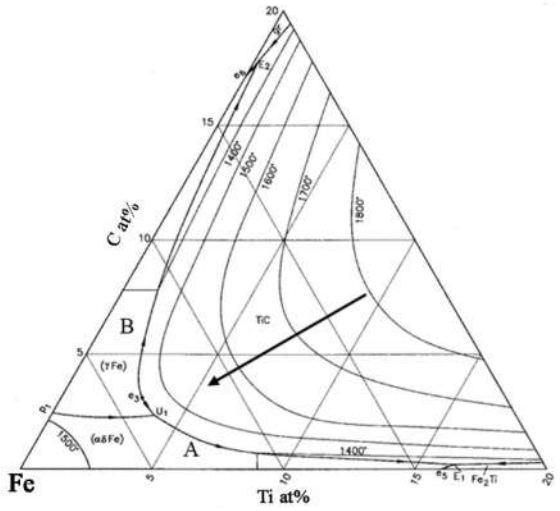

Fig. 5. The liquidus projection of Fe-Ti-C phase diagram in the Fe rich corner [35]

3.2. The effects of mechanical activation on precursor and coating

The images of initial ilmenite powder and the blended mixture after 100 hours of milling can be seen in Figs 6.a and 6.b, respectively. The size of particles became about two orders of magnitude smaller. This refinement exponentially increases the contact area between mixed graphite and ilmenite phases, which decrease the length of diffusion. This can be an important factor in the reduction of ilmenite during a fast process such as laser treatment. However, the decrease in particle size may not be sufficient for complete carbothermic reduction. As will be discussed, mechanical activation and accumulation of crystalline defects have a supplementary effect. The XRD patterns of the powder mixtures activated for 5, 50, 100, and 200 hours are shown in Fig. 7.a. It can be seen that by milling the precursor up to 200 hours, no new peak emerged and therefore no important mechanochemical reaction occurred between ilmenite and graphite. On the other hand, the milling process can dramatically affect the microstructure of existing phases. The increase of activation time resulted in a decrease in the intensity of the graphite main peak, which can be due to partial amorphization. The changes in ilmenite main peak are displayed in Fig. 7.b. It can be seen that by increasing activation time the peak's intensity was decreased and it became wider simultaneously, which is a sign of grain refinement and/or increase of internal microstrain [36].

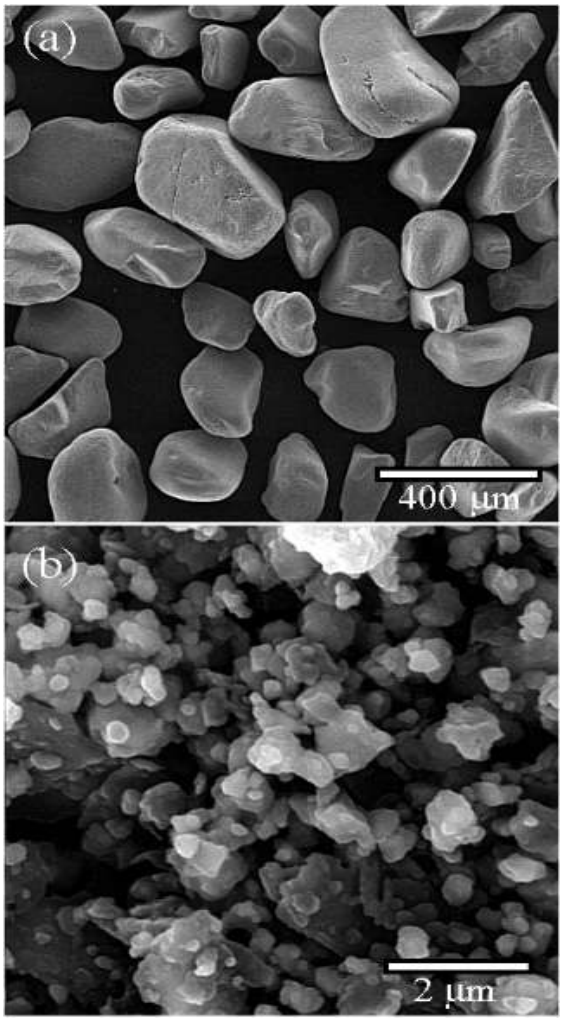

Fig. 6. (a) The initial ilmenite powder
(b) The mixture of graphite and ilmenite with the molar ratio of 8 after 100 hours of milling

[Downloaded from transjour.iust.ac.ir on 2025-05-28]

[DOI: 10.22068/ijmse.16.3.75]

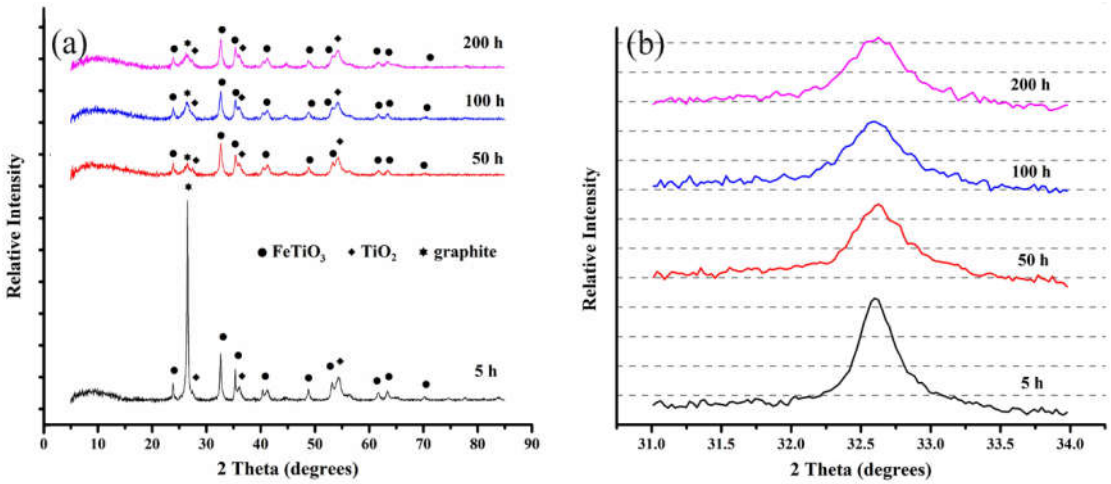

Fig. 7. (a) X-ray diffraction patterns of the mixture of graphite and ilmenite powders at the molar ratio of 8, activated for 5, 50, 100 and 200 hours (b) Changes in the shape of ilmenite main peak by the increase in the milling time

Besides the mentioned decrease in particle size (Fig. 6), the increase in milling time resulted in refinement of crystalline domains inside each particle. Scherer [37] and Williamson-Hall [38] methods were used to calculate the size of crystalline domains and lattice microstrain of ilmenite. The variations of crystallite size versus activation time are plotted in Fig. 8.a. The minimum domain size was somewhat in agreement with that reported by Li and co-workers [39] using Rietveld refinement. (It should be mentioned that the results of various X-ray diffraction line analysis methods may be somehow different [40].) The developed network of grain and subgrain boundaries can act as easy diffusion paths of carbon. On the other hand, ball milling resulted in an increase of lattice microstrain (Fig. 8.b), which is calculated by the Williamson-Hall method. This indicates the accumulation of lattice defects in ilmenite crystallites. The increase of crystalline defects in ilmenite and amorphization of graphite results in a rise in their internal energy level [41], which makes them more reactive.

As could be seen in previous SEM images, the uniformity of particle distribution in the coatings with 100 hours of milling was not completely satisfactory. Micrographs of coatings with 5 and 50 hours of mechanical activation can be seen in Figs 9.a and 9.b, respectively. As is seen, large agglomerations of embedded particles exist. Conversely,

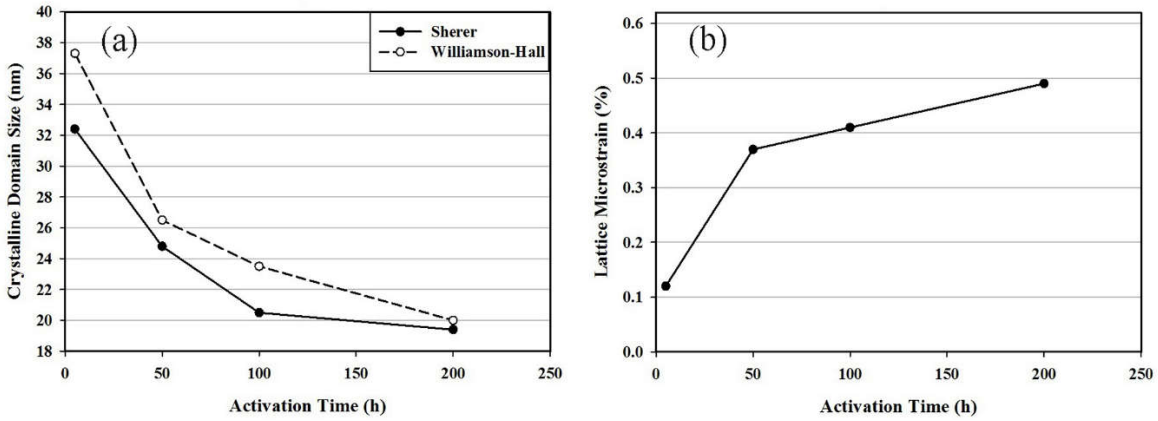

Fig. 8. The effects of the increase in the mechanical activation time on (a) ilmenite crystalline domain size (b) ilmenite lattice microstrain

[Downloaded from transjour.iust.ac.ir on 2025-05-28]

[DOI: 10.22068/ijmse.16.3.75]

SEM investigations showed that the clusters of particle were relatively fewer in sample 8-200. A low magnification image showing the distribution of particles in this sample can be seen in Fig. 9.c, while an image with relatively higher details is presented in Fig. 9.d. The improvement of the homogeneity of distribution of particles can be due to better grinding and mixing of the reaction agents, besides the mentioned changes in diffusion paths and particles internal energies.

Microstructural aspects of the final coating in sample 8-200 can be seen in Fig. 10. A series of solidification microstructures can be detected in Fig. 10. a. Planar, cellular, dendritic, and eutectic regions were formed from the substrate interface toward the coating surface. The fine lamellar structure of eutectic region near the top surface is shown in Fig. 10.b. It is obvious that TiC particles with different morphologies are embedded in this lamellar matrix. The formation of the eutectic region can be a consequence of directional solidification, in which carbon and other solute atoms were rejected from the solidification front toward the surface. Development of the eutectic microstructure (structure of white cast iron) is in agreement with a previous study on laser-surface alloying of iron with graphite [42]. However, it is not possible to completely eliminate the clusters. This may be due to the high speed of LST which does not allow sufficient convection in the melt pool. Round shapes were observed at the boundary of some clusters, as can be seen in Fig. 10.c. Emamian and co-workers stated that rapid temperature reduction can cause a semi-solid region in the Fe-Ti-C melt pool [43]. Therefore, the round shape of boundaries can be a result of fluid flow around the clusters, which was not sufficient to completely dissolve them.

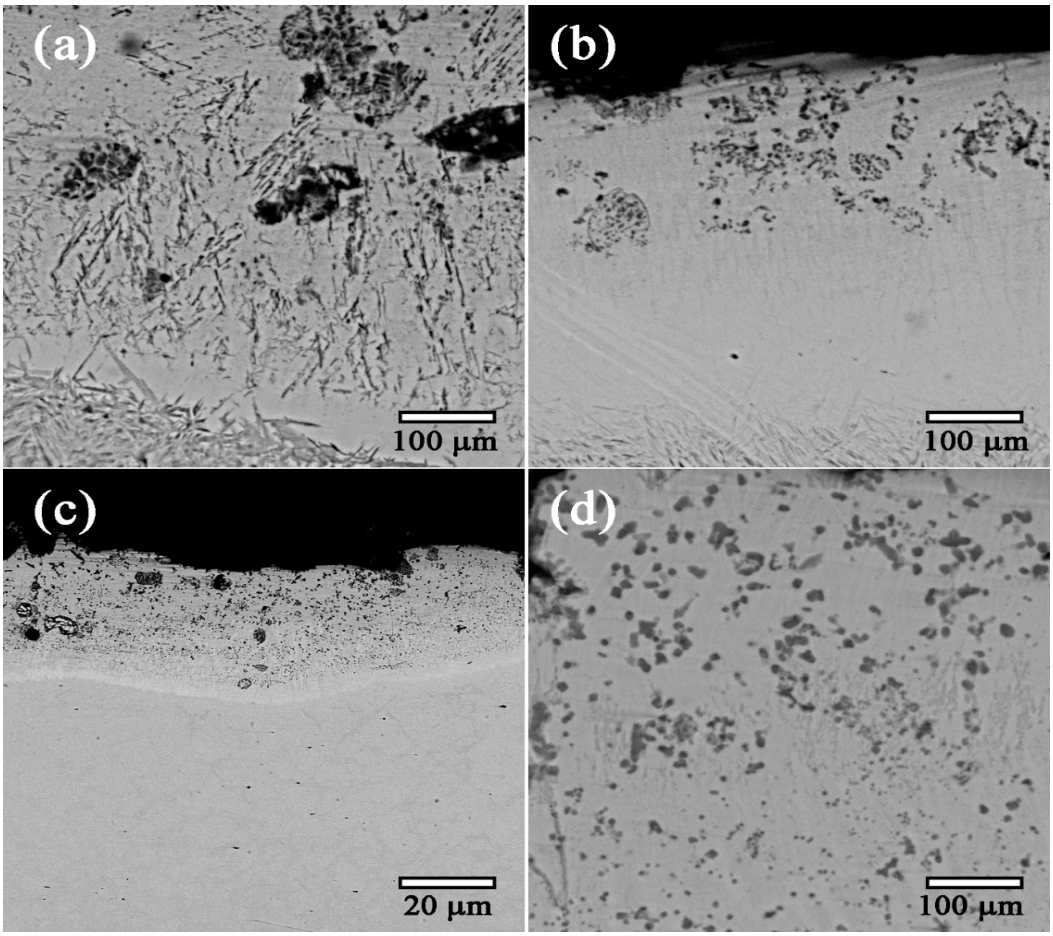

Fig. 9. BSE images showing the distribution of particles in
(a) sample 8-5 (b) sample 8-50 (c) sample 8-200 (d) sample 8-200

[Downloaded from transjour.iust.ac.ir on 2025-05-28]

[DOI: 10.22068/ijmse.16.3.75]

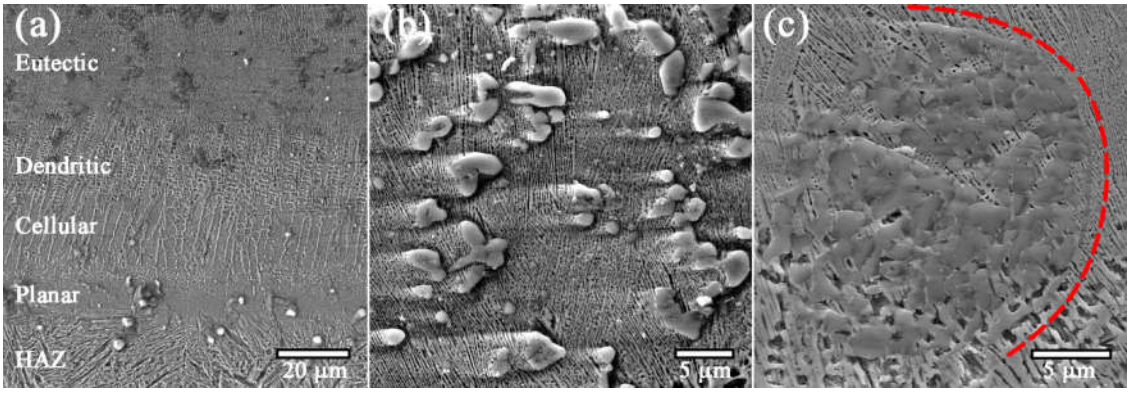

Fig. 10. FESEM images of sample 8-200 (a) General microstructure and its regions (b) particles and matrix in the eutectic section of coating (c) a cluster of particles

Besides the precursor powder, the effects of mechanical activation on the coatings were studied via XRD analysis. Fig. 11 shows the XRD profiles of the coatings which were synthesized from powders by the minimum and the maximum applied activation times. It can be clearly seen that the intensity of TiC peaks was increased. There was also a small shift in the position of peaks. Holt and Munir [44] reported that the increase of carbon content in TiCx from 0.5 to 0.91, increases the cubic lattice parameter from 4.299 to 4.329 Angstroms. Saidi and co-workers [45] also reported an increase from 4.321 to 4.328 Å by increase of x from 0.65 to 0.90. The lattice parameters of samples 8-5 and 8-200 were calculated to be 4.3214 and 4.3254 Angstroms, by Bragg's law [36]. It can be concluded that the carbon content of TiCx particles in this study was increased from about 0.65 to about 0.80. The increase of C/Ti ratio can mean that the dissolution of oxygen in titanium carbide lattice is decreased. This phenomenon implies more progress in the steps of reduction.

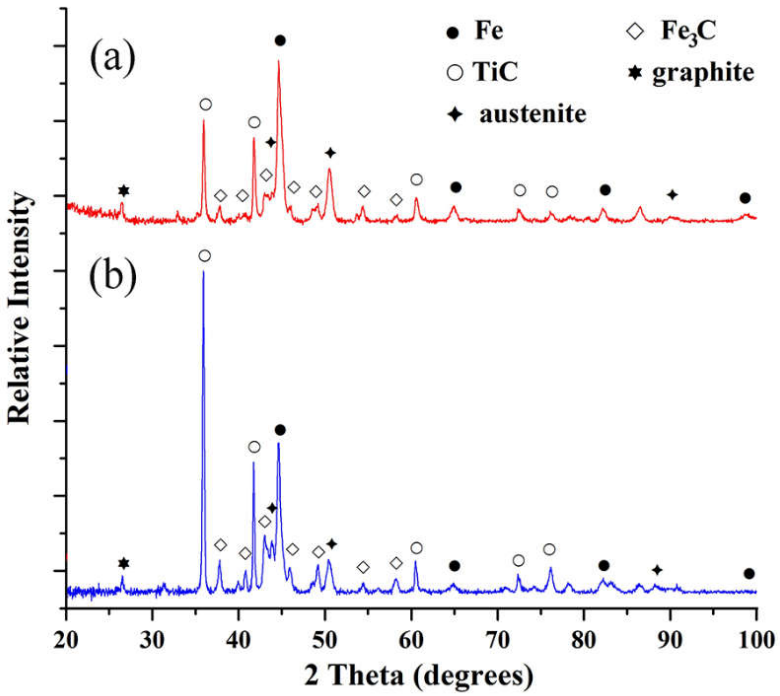

Fig. 11. XRD pattern of the coatings formed from the powder mixtures with a molar ratio of 8, (a) sample 8-5 (b) sample 8-200

[Downloaded from transjour.iust.ac.ir on 2025-05-28]

[DOI: 10.22068/ijmse.16.3.75]

3.3. Microhardness of coatings

Finally, the microhardness measurements were applied to study the effect of excess graphite and mechanical activation on the mechanical properties of the coatings. In sample 4-100, the hardness at regions that were free of synthesized particles was about 550 HV, which can be a result of the martensitic matrix. It was hard to find regions with no embedded particles in sample 8-100. Therefore, the minimum hardness was measured in regions with the lowest density of particles, which was about 800 HV. This increase can be due to the existence of small particles of cementite, besides TiC particles. On the other hand, the maximum values of hardness (in regions with a high density of embedded particles) were measured and presented in Fig. 12.a. The increase of hardness of clustered regions by increase of graphite concentration can imply a rise in the proportion of TiC particles in clusters, rather than oxide phases. This is in agreement with the analysis of XRD profiles. On the other hand, it can be seen in Fig. 12.b that the increase of milling time resulted in the continuous increase of average microhardness of coatings. This can be due to an increase in the proportion of carbide particles which also have higher C/Ti ratio. Conversely, the maximum hardness remained almost constant after 100 hours of mechanical activation, while the difference between the maximum and average hardness is decreased. This can mean that the microstructure of the coating became more uniform. This can also confirm the positive effect of prolonged mechanical activation on the uniformity of particle distribution.

4. CONCLUSIONS

The Fe-TiC composite coating is synthesized on AISI 1020 steel in this research. In-situ synthesis of TiC particles was conducted by carbothermic reduction of ilmenite via laser surface treatment. The mechanical activation of ilmenite-graphite powder mixture was also applied prior to the coating process. It was determined that the ilmenite reduction did not accomplish at graphite to ilmenite molar ratio of 4, which is the stoichiometric ratio. The increase of driving force by mechanical activation was not sufficient for the completion of the reduction during laser surface treatment, as well. The process was improved by the increase of the molar ratio to 6 and was completed at the molar ratio of 8. Consequently, the average microhardness of coatings improved to more than 1300 HV. On the other hand, by mechanical activation of powder mixture for 200 hours in an attritor ball mill, notable improvement is achieved on the uniformity of distribution of reinforcing particles. In this way, a hard coating with TiC reinforcing particles is synthesized by a novel in-situ route.

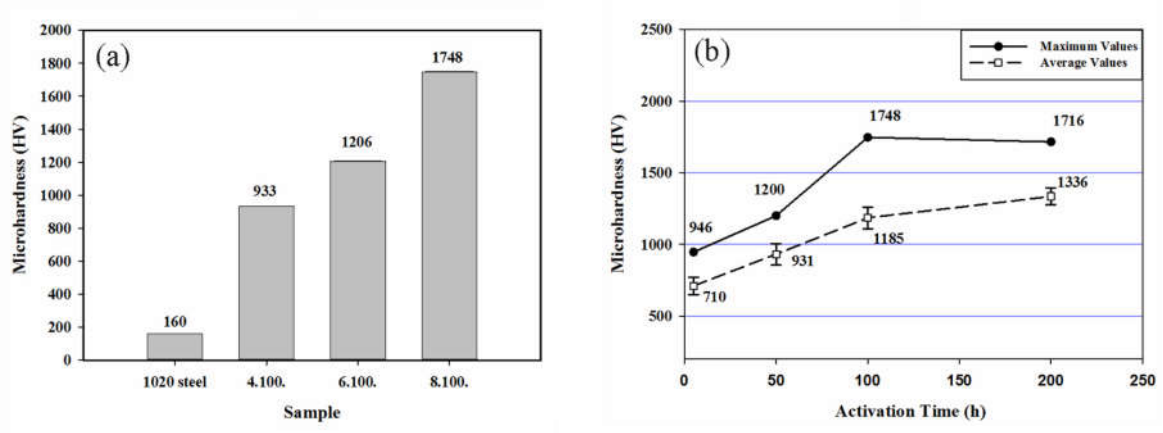

Fig. 12. (a) The hardness of substrate and variations of maximum microhardness of coatings by the increase of ilmenite/graphite molar ratio (b) The variations of maximum and average microhardness of the coatings by the increase in the mechanical activation time

[Downloaded from transjour.iust.ac.ir on 2025-05-28]

[DOI: 10.22068/ijmse.16.3.75]

REFERENCES

1. Bunshah, R.F., Handbook of hard coatings. Noyes Publications / William Andrew Publishing, New York, USA, 2001, 517-533.
2. Sarin, V., "Comprehensive hard materials". Newnes, Oxford, UK, 2004, 20-22.
3. Das, K., Bandyopadhyay, T., Das, S., "A review on the various synthesis routes of TiC reinforced ferrous based composites". J. Mater. Sci., 2002, 37, 3881-3892.
4. Degnan, C. and Shipway P. H., "A comparison of the reciprocating sliding wear behaviour of steel based metal matrix composites processed from self-propagating high-temperature synthesised Fe–TiC and Fe–TiB_2 masteralloys". Wear, 2002, 252, 832-841.
5. Parashivamurthy, K. I., Kumar, R. K., Seetharamu, S. and Chandrasekharaiah, M. N., "Review on TiC reinforced steel composites". J. Mater. Sci., 2001, 36, 4519-4530.
6. Brown, I., Owers, W., "Fabrication microstructure and properties of Fe–TiC ceramic–metal composites". Curr. Appl. Phys., 2004, 4, 171-174.
7. Qu, S., Wang, X., Zhang, M., Zou, Z., "Microstructure and wear properties of Fe–TiC surface composite coating by laser cladding". J. Mater. Sci., 2008, 43, 1546-1551.
8. Rokanopoulou, A., Papadimitriou, G., "Titanium carbide/duplex stainless steel (DSS) metal matrix composite coatings prepared by the plasma transferred arc (PTA) technique: microstructure and wear properties". JCTR, 2011, 8, 427-437.
9. Licheri, R., Orrù, R., Cao, G., Crippa, A., Scholz, R., "Self-propagating combustion synthesis and plasma spraying deposition of TiC–Fe powders". Ceram. Int., 2003, 29, 519-526.
10. Jones, M., Horlock, A., Shipway, P., McCartney, D. G., Wood, J. V., "Microstructure and abrasive wear behaviour of FeCr–TiC coatings deposited by HVOF spraying of SHS powders". Wear, 2011, 249, 246-253.
11. Surzhenkov, A., Antonov, M., Goljandin, D., Kulu, P., Viljus, M., Traksmaa, R., Mere, A., "High-temperature erosion of Fe-based coatings reinforced with cermet particles". Surf. Eng., 2016, 32, 624-630.
12. Lee, J., Euh, K., Oh, J. C., Lee, S., "Microstructure and hardness improvement of TiC/stainless steel surface composites fabricated by high-energy electron beam irradiation". Mater. Sci. Eng, 2002, 323, 251-259.
13. Sahoo, C. K., Masanta, M., "Microstructure and mechanical properties of TiC-Ni coating on AISI304 steel produced by TIG cladding process". J. Mater. Process. Tech., 2017, 240, 126-137.
14. Md Idriss, A. N., Maleque, M. A., Yaacob, I. I., Nasir, R. M., Mridha, S., Baker, T. N., "Wear behaviour at 600°C of surface engineered low-alloy steel containing TiC particles". Mater. Sci. tech., 2017, 33, 1-8.
15. Liu, H., Huang, J., "Reactive thermal spraying of TiC-Fe composite coating by using asphalt as carbonaceous precursor". J. Mater. Sci., 2005, 40, 4149-4151.
16. Toyserkani, E., Khajepour, A., Corbin, S. F., "Laser cladding". CRC press, Florida, USA, 2004.
17. Fan, D., Zhang, J. B., Sun, Y. N., Dai, J. J., Fu, R., "In Situ Formation of TiC Reinforced Intermetallic-Matrix Composite Layers Produced by Laser Cladding". Key. Eng. Mat., 2007, 336, 1380-1382.
18. Muvvala, G., Patra Karmakar, D., Nath A. K., "In-process detection of microstructural changes in laser cladding of in-situ Inconel 718/TiC metal matrix composite coating". J. Alloy. Compd., 2018, 740, 545-558.
19. Hamedi, M. J., Torkamany, M. J., Sabbaghzadeh, J., "Effect of pulsed laser parameters on in-situ TiC synthesis in laser surface treatment". Opt. Laser. Eng., 2011, 49, 557-563.
20. Emamian, A., Corbin, S. F., Khajepour, A., "Effect of laser cladding process parameters on clad quality and in-situ formed microstructure of Fe–TiC composite coatings". Surf. Coat. Tech., 2010, 205, 2007-2015.
21. Razavi, M., Rahimpour, M. R., Ganji, M., Ganjali, M., Gangali, M., "In situ deposition of Fe-TiC nanocomposite on steel by laser cladding". Surf. Rev. Lett., 2017, 24, 1750080.
22. Zhao, G., Zou, Y., Zou, Z. D., Zhang, H., "Research on in situ synthesised (Ti,V)C/Fe composite coating by laser cladding". J. Mater. Sci. Technol., 2015, 31, 1329-1334.
23. Razavi, M., Yaghmaee, M. S., Rahimipour, M. R., Razavi-Tousi, S. S., "The effect of production method on properties of Fe–TiC composite". Int. J. Miner. Process., 2010, 94, 97-100.
24. Wang, Z., Lin, T., He, X., Shao, H., Zheng, J., Qu, X., "Microstructure and properties of TiC-high manganese steel cermet prepared by different sintering processes". J. Alloy. Compd., 2015, 650 918-924.
25. Lahouel, A., Boudebane, S., Iost A., Montagne, A., "A new method to fabricate Fe-TiC composite using conventional sintering and steam hammer". Int. J. Eng. Res. Afr., 2017, 29, 28-44.

[Downloaded from transjour.iust.ac.ir on 2025-05-28]

[DOI: 10.22068/ijmse.16.3.75]

26. Wang, Y. M., Yuan, Z. F., Guo, Z. C., Tan, Q. Q., Li, Z. Y., Jiang, W. Z., "Reduction mechanism of natural ilmenite with graphite". Trans. Nonferrous Met. Soc. China, 2008, 18, 962-968.
27. Khalili, A., Goodarzi, M., Mojtahedi, M., Torkamany, M. J., "Solidification microstructure of in-situ laser-synthesized Fe-TiC hard coating". Surf. Coat. Tech., 2016, 307, 747-752.
28. Dewan, M. A., Zhang, G., Ostrovski, O., "Phase development in carbothermal reduction of ilmenite concentrates and synthetic rutile". ISIJ international, 2010, 50, 647-653.
29. Zhang, H., Zou, Y., Zou, Z., Wu, D., "Microstructures and properties of low-chromium high corrosion-resistant TiC–VC reinforced Fe-based laser cladding layer". J. Alloy. Compd., 2015, 622, 62-68.
30. Kurz, W., Fisher, D. J., "Fundamentals of Solidification". Trans Tech Publications, Switzerland, 1992, 50-55.
31. Chen, S., Chen, X., Wang, L., Liang, J., Liu, C., "Laser cladding FeCrCoNiTiAl high entropy alloy coatings reinforced with self-generated TiC particles". J. Laser Appl., 2017, 29, 012004-8.
32. Hao, M., Sun, Y., "A FEM model for simulating temperature field in coaxial laser cladding of Ti6Al4V alloy using an inverse modeling approach". Int. J. Heat. Mass. Tran., 2013, 64, 352-360.
33. Lei, Y., Sun, R., Tang, Y., Niu, W., "Numerical simulation of temperature distribution and TiC growth kinetics for high power laser clad TiC/NiCrBSiC composite coatings". Opt. Laser. Technol., 2012, 44, 1141-1147.
34. Savvatimskiy, A. I., "Measurements of the melting point of graphite and the properties of liquid carbon", (a review for 1963–2003). Carbon, 2005, 43, 1115-1142.
35. Jonsson, S., "Assessment of the Fe-Ti-C system, calculation of the Fe-TiN system, and prediction of the solubility limit of Ti(C,N) in liquid Fe". Metall and Materi Trans B, 1998, 29 (2) 371-384
36. Cullity, B. D., "Elements of X-Ray Diffraction". 2nd ed. Addison-Wesley, 1978, 95-105.
37. Scherrer, P., "Estimation of the size and internal structure of colloidal particles by means of röntgen. Nachr Ges Wiss Göttingen", 1918, 2, 96-100.
38. Williamson, G. K., Hall W. H., "X-ray line broadening from filed aluminium and wolfram". Acta. Metall., 1953, 1, 22-31.
39. Li, C., Liang, B., Guo, L. H., Wu, Z. B., "Effect of mechanical activation on the dissolution of Panzhihua ilmenite". Miner. Eng., 2006, 19, 1430-1438.
40. Soleimanian, V., Mojtahedi, M., "A comparison between different X-ray diffraction line broadening analysis methods for nanocrystalline ball-milled FCC powders". Appl. Phys. A., 2015, 119, 977-987.
41. Suryanarayana, C., "Mechanical alloying and milling". Marcel Dekker, New York , 2004, 139-156.
42. Walker, A., Flower, H., West, D., "The laser surface-alloying of iron with carbon". J. Mater. Sci., 1985, 20, 989-995.
43. Emamian, A., Corbin, S. F., Khajepour, A., "In-Situ Deposition of Metal Matrix Composite in Fe-Ti-C System Using Laser Cladding Process", In: Metal. Ceramic and Polymeric Composites for Various Uses. editor: Cuppoletti, J., InTech, 2011. pages?
44. Holt, J. B., Munir, Z. A., "Combustion synthesis of titanium carbide: Theory and experiment". J. Mater. Sci.,1986, 21, 251-259.
45. Saidi, A., Chrysanthou, A., Wood, J. V., Kellie, J. L. F., "Preparation of Fe-TiC composites by the thermal-explosion mode of combustion synthesis". Ceramics International, 1997, 23, 185-189.

[Downloaded from transjour.iust.ac.ir on 2025-05-28]

[DOI: 10.22068/ijmse.16.3.75]